AD-A134 700 NUMERICAL SIMULATION OF FLOW OVER ROUGH SURFACES INCLUDING EFFECTS OF SHO..(U) SCIENCE APPLICATIONS INC WAYNE PA G H CHRISTOPH ET AL. AUG 83 SAI-067-84R-001 1/1

UNCLASSIFIED AFWAL-TR-83-3071 F33615-82-M-3029 F/G 20/4 NL

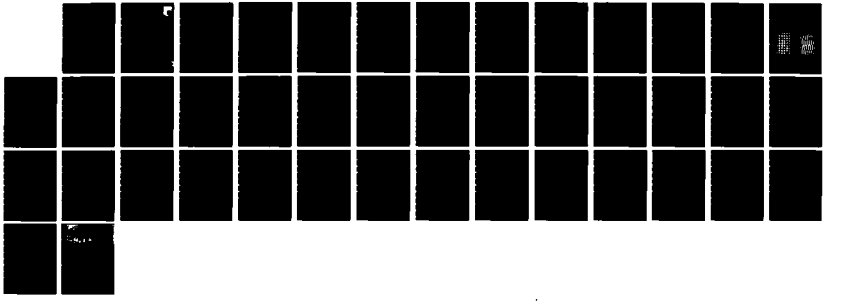

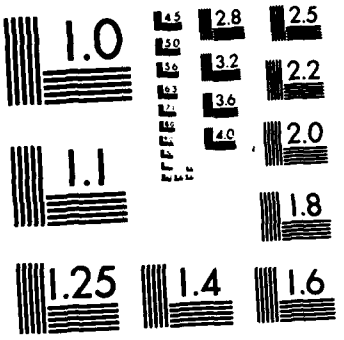

(10)

AD-A134700

AFWAL-TR-83-3071

NUMERICAL SIMULATION OF FLOW OVER ROUGH SURFACES, INCLUDING EFFECTS OF SHOCK WAVES

G. H. Christoph

Science Applications, Inc.
Wayne, Pennsylvania 19087

and

Anthony W. Fiore
Aeromechanics Division
Flight Dynamics Laboratory

August 1983

Final Report for Period August 1982 to January 1983

Approved for public release; distribution unlimited.

DTIC FILE COPY

FLIGHT DYNAMICS LABORATORY
AIR FORCE WRIGHT AERONAUTICAL LABORATORIES
AIR FORCE SYSTEMS COMMAND
WRIGHT-PATTERSON AIR FORCE BASE, OHIO 45433

NOTICE

When Government drawings, specifications, or other data are used for any purpose other than in connection with a definitely related Government procurement operation, the United States Government thereby incurs no responsibility nor any obligation whatsoever; and the fact that the government may have formulated, furnished, or in any way supplied the said drawings, specifications, or other data, is not to be regarded by implication or otherwise as in any manner licensing the holder or any other person or corporation, or conveying any rights or permission to manufacture use, or sell any patented invention that may in any way be related thereto.

This report has been reviewed by the Office of Public Affairs (ASD/PA) and is releasable to the National Technical Information Service (NTIS). At NTIS, it will be available to the general public, including foreign nations.

This technical report has been reviewed and is approved for publication.

Anthony W. Fiore

ANTHONY W. FIORE
Project Engineer
High Speed Aerodynamics Group

J. Christopher Boison

J. CHRISTOPHER BOISON
Chief, High Speed Aero. Perf. Br.
Aeromechanics Division

FOR THE COMMANDER

Ralph W Holm

RALPH W. HOLM
COLONEL, USAF
Chief, Aeromechanics Division

"If your address has changed, if you wish to be removed from our mailing list, or if the addressee is no longer employed by your organization please notify AFWAL/FIMG *W-PAFB, OH 45433 to help us maintain a current mailing list".*

Copies of this report should not be returned unless return is required by security considerations, contractual obligations, or notice on a specific document.

UNCLASSIFIED

SECURITY CLASSIFICATION OF THIS PAGE (When Data Entered)

REPORT DOCUMENTATION PAGE		READ INSTRUCTIONS BEFORE COMPLETING FORM
1. REPORT NUMBER AFWAL-TR-83-3071	2. GOVT ACCESSION NO. AD-A134 700	3. RECIPIENT'S CATALOG NUMBER
4. TITLE (and Subtitle) NUMERICAL SIMULATION OF FLOW OVER ROUGH SURFACES, INCLUDING EFFECTS OF SHOCK WAVES		5. TYPE OF REPORT & PERIOD COVERED Final Report August 1982 to January 1983
		6. PERFORMING ORG. REPORT NUMBER SAI-067-84R-001
7. AUTHOR(s) George H. Christoph, Science Applications, Inc. and Anthony W. Fiore, AFWAL/FIMG		8. CONTRACT OR GRANT NUMBER(s) F33615-82-M-3029
9. PERFORMING ORGANIZATION NAME AND ADDRESS Science Applications, Inc. 994 Old Eagle School Road, Suite 1018 Wayne, Pennsylvania 19087		10. PROGRAM ELEMENT, PROJECT, TASK AREA & WORK UNIT NUMBERS 2307N455
11. CONTROLLING OFFICE NAME AND ADDRESS Aeromechanics Division Flight Dynamics Laboratory WPAFB, Ohio 45435		12. REPORT DATE August 1983 13. NUMBER OF PAGES 37
14. MONITORING AGENCY NAME & ADDRESS(if different from Controlling Office) Air Force Wright Aeronautical Laboratories Air Force Systems Command Wright Patterson Air Force Base, Ohio 45433		15. SECURITY CLASS. (of this report) UNCLASSIFIED 15a. DECLASSIFICATION/DOWNGRADING SCHEDULE N/A

16. DISTRIBUTION STATEMENT (of this Report)

Approved for public release; distribution unlimited.

17. DISTRIBUTION STATEMENT (of the abstract entered in Block 20, if different from Report)

18. SUPPLEMENTARY NOTES

19. KEY WORDS (Continue on reverse side if necessary and identify by block number)

Boundary Layers
Surface Roughness
Finite Difference
Turbulence Modeling
Compressible Flow
Skin Friction
Shock Wave

20. ABSTRACT (Continue on reverse side if necessary and identify by block number)

The finite-difference boundary layer method of Christoph and Pletcher for flow over rough surfaces is extended to include the effect of shock waves off roughness elements. The equivalent sand-grain roughness height is not needed, but rather the actual roughness height and spacing is used. A turbulence model that contains very little empiricism but yet is capable of accounting for roughness height, spacing, and geometry is presented. → cont'd

(Over)

DD FORM 1 JAN 73 1473 EDITION OF 1 NOV 65 IS OBSOLETE

UNCLASSIFIED

SECURITY CLASSIFICATION OF THIS PAGE (When Data Entered)

cont > Computations are presented for smooth and rough wall profiles and skin friction data obtained at AFWAL in the Mach 6 facility. Agreement is quite good, especially in light of the fact that in no way was the turbulence modeling adjusted during these comparisons.

PREFACE

This final technical report was prepared under Contract F33615-82-M-3029, "Numerical Simulation of Flow Over Rough Surfaces." The work was administered by the Air Force Flight Dynamics Laboratory, Wright-Patterson Air Force Base, Ohio, Dr. Anthony W. Fiore (FIMG), Project Engineer. This investigation was conducted in the time period September 1982 to March 1983, and the final report was submitted in March 1983.

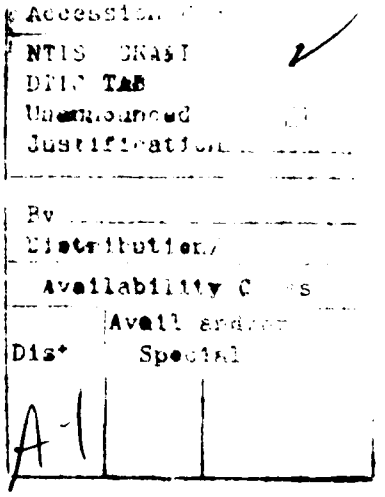

TABLE OF CONTENTS

LIST OF ILLUSTRATIONS

LIST OF TABLES

LIST OF SYMBOLS

A^+	Van Driest constant, = 26
$B(y)$	Function defined by Eq. (11)
c_D	Form-drag coefficient
c_f	Skin-friction coefficient, = $2\ \tau_w/(\rho_e u_e^2)$
$D(y)$	Roughness element width
D_a	Viscous damping function
$f(y)$	Function defined by Eq. (11)
F	Variable defined by Eq. (7)
h	Static enthalpy
H	Total enthalpy, = $h + u^2/2$
I	Variable defined by Eq. (7)
k	Thermal conductivity
K	Roughness height
K_{es}	Equivalent sand-grain roughness height
K^+	= Ku^*/ν_w
ℓ	Mixing length
L	Roughness element spacing
M	Mach number
P	Static pressure
P_o	Total pressure
Pr	Prandtl number
$\dot{q}$	Heat flux
Re_x	$u_e x/\nu_e$
Re_θ	= $u_e \theta/\nu_e$
RFP	Rough flat plate

S	Entropy
SFP	Smooth flat plate
St	Stanton number, $= \dot{q}_w/[\rho_e u_e (h_{aw} - h_w)]$
T	Temperature
T_o	Total temperature
u	Streamwise velocity
u^*	Friction velocity, $= (\tau_w/\rho_w)^{1/2}$
u^+	$= u/u^*$
v	Normal velocity
$\tilde{v}$	Normal velocity, $= (\rho v + \overline{\rho' v'})/\rho$
V	Variable defined by Eq. (7)
x	Length measured from leading edge
y	Coordinate normal to x
y^+	$= yu^*/\nu_w$
z	Function defined by Eq. (23)
δ	Boundary-layer thickness
η	Transformed normal coordinate defined by Eq. (6)
θ	Momentum thickness
μ	Viscosity
ν	Kinematic viscosity
ρ	Density
τ	Shear stress

Subscripts

aw	Adiabatic wall
e	Edge
i	Inner
o	Outer
r	Rough
s	Smooth
t	Turbulent
w	Wall
FT	Fully turbulent
∞	Freestream

Superscripts

$( )'$	Primes denote fluctuating quantities
$(\bar{})$	Bars denote time mean quantities

SECTION I

INTRODUCTION

The impetus for the present study was a series of roughness experiments conducted in the AFWAL Mach 6 facility. These experiments were to examine roughness induced shock vorticity effects on boundary layer structure. Two types of roughness patterns will be investigated: a square shape and a diamond shape. These patterns were obtained by machining grooves in a smooth flat plate, as depicted in Figure 1. The square elements will produce a detached shock resulting in variable vorticity, while the diamond elements will have attached shocks and constant vorticity. As of the writing of this report, only the square shaped pattern has been tested. The roughness elements are 0.02 inches high by 0.04 inches on each side with center-to-center spacings of 0.08 inches.

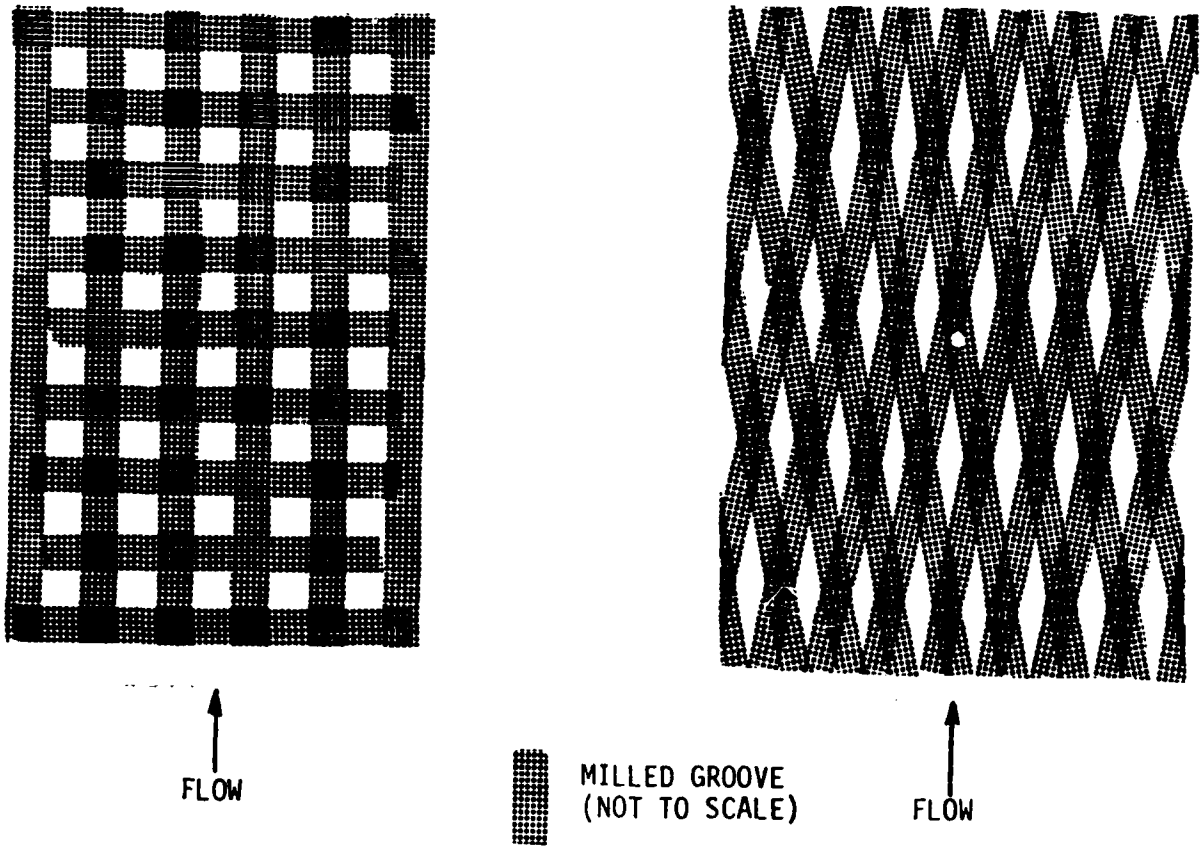

FIGURE 1. SQUARE AND DIAMOND SHAPED ROUGHNESS PATTERNS

Due to the thin boundary layer at high Mach numbers, it is extremely difficult to make detailed flow measurements. Furthermore, in hypersonic flow at high Reynolds number, most of the boundary layer is supersonic. In fact, even small roughness elements can generate shocklets. If these shocklets are curved, due to the shape of the elements, vorticity will be added to the flow and turbulent quantities such as the boundary layer growth rate will be affected. Because of the need to simulate Mach number and shock generated vorticity effects for rough surfaces, one does not have the luxury of scaling up roughness elements as can be done, for example, in an environmental wind tunnel.

On the other hand, detailed flow calculations can be performed over a rough surface, even for small elements in thin boundary layers. Such parameters as Mach number, wall temperature, and pressure gradient can be easily simulated. Profiles, skin-friction and heat transfer coefficients, and fluctuating turbulent quantities can be calculated. One can also examine different roughness element geometries with attached and detached shocks to see how vorticity and momentum defects influence boundary layer structure.

Most roughness analyses are based on Nikuradse's sand-grain experiments and the "law of the wall" velocity profiles fit to the data. Several correlations have been proposed to relate real roughness heights, spacings, and geometries to an equivalent sand-grain roughness height so Nikuradse's data can be used. Examples of such correlations can be found in Betterman[1], Dirling[2], and White and Grabow[3]. However, the general applicability of such correlations is unknown. More recently, surface roughness calculations have been performed by differential methods. Cebeci and Chang[4] numerically solved the incompressible boundary layer equations employing an algebraic eddy-viscosity formulation modified for surface roughness. This modification was based on Rotta's model[5], which displaces the normal coordinate of the rough wall velocity profile. An expression for this displacement, and the resulting mixing length, is given by Cebeci and Chang as a function of an equivalent sand-grain roughness height.

Emphasizing compressible flows for a variety of edge and wall conditions, Hodge and Adams[6] numerically solved the boundary layer equations and an integral form of the kinetic-energy-of-turbulence equation. Roughness effects were accounted for by a form-drag term in the momentum equation and by modifications, based on the results of Healzer et al.[7], for several of the nine empirical constants. It is the intent of this study to utilize a numerical technique for calculating skin friction and heat transfer over surfaces with real roughness, including the effect of shock waves, using as little empiricism as possible.

Contriving an equivalent sand-grain roughness height for real roughness heights, spacings, and geometries is not very satisfying. A physically more meaningful method that accounts for actual roughness effects is that employed by Finson and Clarke[8], Lin and Bywater[9], and Christoph and Pletcher[10]. These techniques calculate the form-drag contributions of individual elements. Roughness elements are assumed to occupy no physical space. The governing boundary layer equations are cast in a form to account for the blockage effects of the roughness elements. Terms that act in the streamwise direction are multiplied by $[1 - D(y)/L]$ where $D(y)$ is the element width at height y and L is the average center-to-center spacing. Terms that act in a direction normal to the streamwise direction are multiplied by $[- D^2(y)/L^2]$. The effect of roughness is described by a sink term in the momentum equation and by a source term in the static enthalpy equation.

When the above approach is adopted, one must examine carefully the turbulence model used. Existing rough wall, mixing-length models are expressed in terms of an equivalent sand-grain roughness height and are validated for boundary layer equations without blockage effects or source and sink terms (e.g., Cebeci and Chang[4] or Healzer et al.[7]). Lin and Bywater[9] modify their turbulent kinetic energy model equation to include blockage effects. Finson and Clarke[8] use a second-order closure approximation for their turbulence model, describing the effect of roughness by distributed source or sink terms in the appropriate equations. These

latter two methods are still left with modeling constants whose roughness effects are uncertain. For the present study, it was decided to use the analysis of Christoph and Pletcher[10] modified to include shock wave effects. In this analysis a two-layer algebraic mixing-length model is employed that explicitly includes roughness height, frequency, and type.

Besides giving an indication of measurement magnitudes to be expected, calculations can assist in designing experiments. Roughness size plus flow parameters can be determined to best simulate flight conditions. It is hoped that computations and experiments progress hand-and-hand to evolve an experimental program that produces useful data for accurate turbulence modeling and a clearer understanding of the flow physics.

SECTION II

EQUATIONS AND SOLUTION PROCEDURES

1. GOVERNING EQUATIONS

For a smooth two-dimensional, steady, compressible turbulent flow, the standard boundary layer equations are

CONTINUITY

$$\frac{\partial}{\partial x}(\rho u) + \frac{\partial}{\partial y}(\rho \tilde{v}) = 0 \tag{1}$$

MOMENTUM

$$\rho u \frac{\partial u}{\partial x} + \rho \tilde{v} \frac{\partial u}{\partial y} = - \frac{dP}{dx} + \frac{\partial}{\partial y}\left(\mu \frac{\partial u}{\partial y} - \overline{\rho v' u'}\right) \tag{2}$$

ENERGY

$$\rho u \frac{\partial H}{\partial x} + \rho \tilde{v} \frac{\partial H}{\partial y} = \frac{\partial}{\partial y}\left(\frac{\mu}{Pr} \frac{\partial H}{\partial y} - \rho \overline{v' h'} + u \left[\left(1 - \frac{1}{Pr}\right) \mu \frac{\partial u}{\partial y} - \rho \overline{v' u'} \right] \right) \tag{3}$$

The coordinate x is measured along the surface from the leading edge and the coordinate y is perpendicular to x. The boundary conditions imposed are at $y = 0$, $u(x,0) = \tilde{v}(x,0) = 0$, $H(x,0) = H_w(x)$ or $(\partial H/\partial y)_{y=0}$ specified, and as $y \to \infty$, $u(x,y) = u_e(x)$ and $H(x,y) = H_e(x)$. In the above, $\tilde{v} = (\rho v + \overline{\rho' v'})/\rho$. The terms $-\overline{\rho v' u'}$ and $\overline{\rho v' h'}$ represent the apparent turbulent shear stress and heat flux, respectively, and must be modeled.

Equations (1) - (3) are now recast, in the manner proposed by Finson and Clarke, to account for roughness. As discussed in the Introduction, terms that act in the streamwise direction are multiplied by [1 - D(y)/L], and terms that act normal to the streamwise direction are multiplied by [1 - $D^2(y)/(L^2)$]. A form-drag term

$$-\frac{1}{2}\rho u^2 c_D D(y)/L^2 \tag{4}$$

is added to the momentum equation, and a source term

$$\frac{1}{2}\rho u^3 c_D D(y)/L^2 \tag{5}$$

is added to the static enthalpy equation such that the total enthalpy is not altered. Also, the coordinates are transformed by

$$x = x, \qquad \eta = \left(\frac{u_e}{\rho_e \mu_e}\right)^{1/2} \int_o^y \rho \, dy \tag{6}$$

and the dependent variables are nondimensionalized according to

$$F = \frac{u}{u_e}, \quad I = \frac{H}{H_e}, \quad V = \rho\tilde{v}\left(\frac{x}{u_e \rho_e \mu_e}\right)^{1/2} + x f(y) F \frac{\partial \eta}{\partial x} \quad . \tag{7}$$

Utilizing Equations (6) and (7) and the roughness modifications, the conservation equations become

CONTINUITY

$$f(y)\frac{\partial}{\partial x}\left[(u_e \rho_e \mu_e x)^{1/2} F\right] + \frac{\partial}{\partial \eta}\left[\left(\frac{u_e \rho_e \mu_e}{x}\right)^{1/2} V\right] = 0 \tag{8}$$

MOMENTUM

$$xf(y)F\frac{\partial F}{\partial x} + V\frac{\partial F}{\partial \eta} = -xf(y)\left(\frac{F^2}{u_e^2}\frac{du_e}{dx} + \frac{1}{\rho u_e^2}\frac{dP}{dx}\right) + \frac{1}{B(y)}\frac{\partial}{\partial \eta}\left(\frac{\rho\,\bar{\mu}\,B(y)}{\rho_e \mu_e}\frac{\partial F}{\partial \eta}\right) - \frac{1}{2}\frac{c_D D(y)\,xF^2}{L^2 B(y)} \tag{9}$$

ENERGY

$$xf(y)F\frac{\partial I}{\partial x} + V\frac{\partial I}{\partial \eta} = \frac{1}{B(y)}\frac{\partial}{\partial \eta}\left\{B(y)\left(\frac{\mu}{Pr} + \frac{\mu_t}{Pr_t}\right)\frac{\rho}{\rho_e\,\mu_e}\frac{\partial I}{\partial \eta} + B(y)\frac{\rho u_e^2 F}{H_e \rho_e \mu_e}\left[\mu\left(1 - \frac{1}{Pr}\right) + \mu_t\left(1 - \frac{1}{Pr_t}\right)\right]\frac{\partial F}{\partial \eta}\right\} \tag{10}$$

The functions B(y) and f(y) are defined by

$$B(y) = 1 - D^2(y)/(L^2) \tag{11}$$

$$f(y) = [1 - D(y)/L]/B(y)$$

In the above, the Boussinesq assumption has been employed to evaluate the shear stress; that is, it has been assumed that

$$\tau = \mu\frac{\partial u}{\partial y} - \rho\overline{v'u'} = (\mu + \mu_t)\frac{\partial u}{\partial y} = \bar{\mu}\frac{\partial u}{\partial y} \tag{12}$$

It has been further assumed that the turbulent heat flux can likewise be represented through the Boussinesq assumption. Representing the turbulent conductivity by

$$k_t = c_p \mu_t / Pr_t \tag{13}$$

where the turbulent Prandtl number was set equal to a constant value of 0.9, the turbulent heat flux can be evaluated as

$$-\rho\overline{v'h'} = \frac{\mu_t}{Pr_t}\frac{\partial h}{\partial y} = \frac{\mu_t}{Pr_t}\frac{\partial H}{\partial y} - \frac{\mu_t}{Pr_t} u \frac{\partial u}{\partial y} \quad . \tag{14}$$

Equations (12) - (14) were employed to eliminate the Reynolds stress and heat flux terms prior to transforming the equations. The boundary conditions for the new variables are given by

$$F(x,0) = 0, \; V(x,0) = 0$$

$$I(x,0) = I_w(x) \text{ or } \left.\frac{\partial I}{\partial \eta}\right|_{\eta=0} \text{ specified}$$

and as

$$\eta \to \infty, \; F = I = 1.0 \quad . \tag{15}$$

In order to include boundary layer edge changes for variable entropy, the pressure gradient is written as

$$-\frac{dP}{dx} = \rho_e u_e \frac{du_e}{dx} + \rho_e T_e \frac{dS_e}{dx} \tag{16}$$

where S is the entropy.

2. TURBULENCE MODELING

Prandtl's mixing-length hypothesis is used to evaluate the apparent turbulent viscosity according to

$$\mu_t = \rho \ell^2 \left| \frac{\partial u}{\partial y} \right| \quad . \tag{17}$$

The mixing length is evaluated as

$$\ell_i = 0.41 \, D_a y \tag{18}$$

in the inner region and

$$\ell_o = 0.089 \, \delta \tag{19}$$

in the outer region where D_a is a modified van Driest damping function and δ is the boundary layer thickness. The damping function and the form of the mixing length, Equation (18), must be specified for such complicating effects as wall transpiration and surface roughness. For incompressible flow over an impermeable smooth wall, van Driest[11] recommended

$$D_a = 1 - \exp(-y^+/A^+) \tag{20}$$

where $A^+ = 26$. Pletcher[12] modified this form for transpired flows by setting

$$D_a = 1 - \exp(-z) \tag{21}$$

where

$$z = \frac{y^+}{26} (\tau/\tau_w)^{1/2} (\tau_{FT}/\tau_w)^{1/2} \tag{22}$$

and τ_{FT} is the shear stress near the beginning of the fully turbulent region. This form for z was proposed to account for shear stress variations near a wall such as occurs with wall blowing or roughness.

If the shear stresses in Equation (22) are rough wall values, one would expect the smooth wall constant, $A^+ = 26$, to change. Instead of trying to find a new empirical constant/function for rough walls, let us try multiplying the right-hand side of Equation (22) by τ_{wr}/τ_{ws} where the subscripts r and s represent rough and smooth values, respectively. Then

$$z = \frac{y^+}{26} (\tau_r/\tau_{wr})^{1/2} (\tau_{FTr}/\tau_{wr})^{1/2} (\tau_{wr}/\tau_{ws}) \quad . \tag{23}$$

An expression for τ_{FTr} is obtained by neglecting the convective acceleration and by evaluating the momentum equation at the top of the roughness elements (y = K). Then

$$\tau_{FTr} = \tau_{ws} + \frac{1}{2}\int_o^K \frac{f(y)\ \rho u^2 c_D D(y)}{B(y)\ L^2}\, dy \tag{24}$$

where the pressure gradient term is neglected. As the roughness height increases, the damping factor D_a approaches one, as expected.

It is also necessary to modify the mixing-length formulation, Equation (18), for roughness effects. Healzer et al.[7] and Cebeci and Chang[4] suggest mixing-length modifications for sand-grain roughness. For the present study, a mixing-length was derived based on the "law of the wall" analysis of White and Christoph[13]. For illustrative purposes, the derivation presented here considers incompressible flow. First, approximate the turbulent shear using Prandtl's mixing-length hypothesis according to Equations (17) and (18). Then, note that near the wall there is negligible convection acceleration, so that an expression for τ_w, such as Equation (24) holds. Combining these results gives an expression for $\partial u^+/\partial y^+$. For fully turbulent flow with roughness, one has

$$\frac{\partial u^+}{\partial y^+} = \frac{\left[\tau_{ws}/\tau_{wr} + \frac{1}{2}\int_0^{K^+} \frac{\nu_w c_D f(y^+) u^{+2} D(y^+)}{u^* L^2 B(y^+)} dy^+ \right]^{1/2}}{0.41\ y^+} \quad . \quad (25)$$

Note that for a smooth wall one would obtain

$$\frac{\partial u^+}{\partial y^+} = \frac{1}{0.41\ y^+} \quad (26)$$

where $\ell = 0.41\ y$. This suggests that for a rough surface

$$\ell = \frac{0.41\ y}{\left[\tau_{ws}/\tau_{wr} + \frac{1}{2}\int_0^{K^+} \frac{\nu_w c_D f(y^+)\ u^{+2} D(y^+)}{u^*\ L^2\ B(y^+)} dy^+ \right]^{1/2}} \quad . \quad (27)$$

For the present study, the rough wall mixing-length was derived to include compressibility. The "law of the wall" profiles outlined above are in reasonable agreement with the roughness channel-flow data of Schlichting[14]. These are given in Reference 10. This is a partial verification for the form of the damping function given in Equation (23) and the mixing-length modification just discussed.

The switch point from the inner [Equation (18)] to the outer [Equation (19)] model was made in accordance with the low Reynolds number modification presented in Reference 15. This provides that the switch be made at the point where ℓ_i first becomes equal to ℓ_o provided that $y^+ \geq 50$. If $y^+ < 50$ when $\ell_i = \ell_o$, then the switch point is delayed until y^+ becomes equal to 50 and ℓ_o becomes equal to ℓ_i at $y^+ = 50$. This prevents the suppression of the fully turbulent portion of the velocity profile that can occur at low values of Re_θ. This effect persists to higher and higher values of Re_θ as the Mach number increases.

3. TREATMENT OF SHOCKS

In a supersonic/hypersonic boundary layer it is possible to generate shocklets even for small roughness heights. The analysis of Christoph and Pletcher[10] was modified to account for the effect of shocklets. To the author's knowledge, the only data available showing shocklets were obtained by A. Fiore of AFWAL . These data for the square pattern of Figure 1, form the basis of the present modifications. Photographs of the shocklets are not shown in this report because they would not reproduce clearly. Qualitatively, the shocks start at the sonic line and are detached, and they approach the flow Mach angle at the boundary layer edge. The axial extent of the shock before merging with the boundary layer edge is approximately equal to the roughness element spacing. A reproduced drawing of the Schlieren is shown below. It is impossible to describe the shock shapes accurately from the available photographs. Instead, the shock shape is calculated by assigning values of M sin θ (code input parameter) where θ is the shock angle.

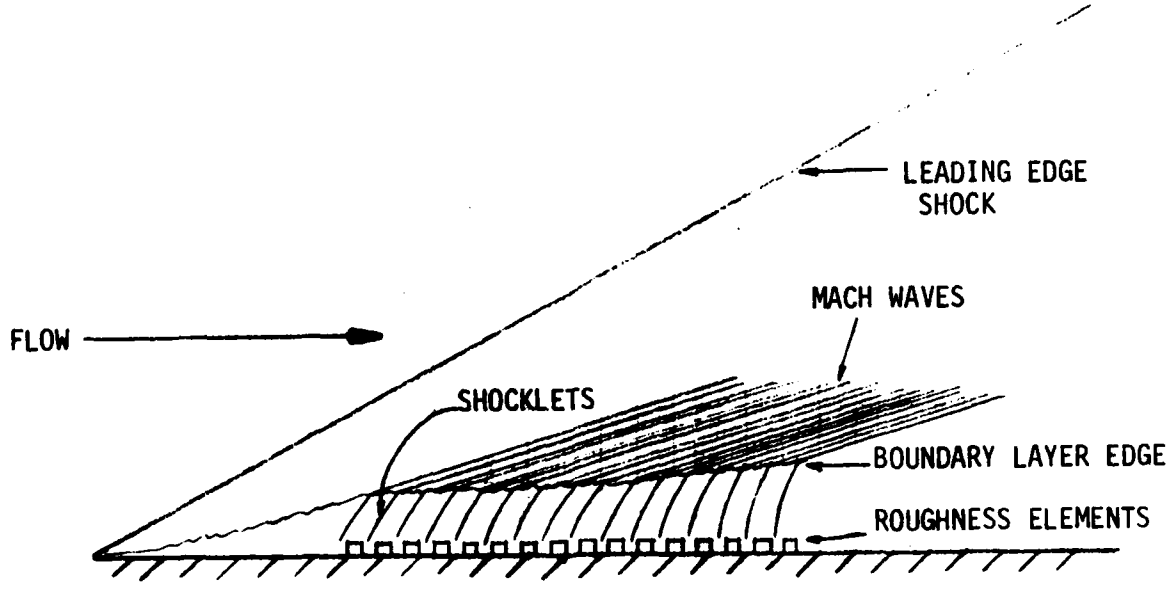

FIGURE 2. SHOCKLETS OFF ROUGHNESS ELEMENTS

It is believed that $M \sin \theta$ is slightly greater than 1.0, i.e., shocks are weak. The reason for this belief is that calculations made without shocks are in reasonably good agreement with profile data (discussed in Results section of this report). Also, from the photographs the shock shape appears invariant in the flow direction. In this study, the shock shape is kept similar at all axial stations, expanding with the growing boundary layer. For determination of the initial shock shape, no shocks are allowed over the first few elements so that a rough wall Mach number distribution through the boundary layer can be determined. Finally, oblique shock relations are used to calculate flow variables behind the shocklets. Because of the uncertainty in the shock angles at the edge of the boundary layer, edge variations of velocity and entropy have been set to zero for the results presented in this report.

4. METHOD OF SOLUTION

Equations (8) - (10) are solved numerically by a fully implicit finite-difference procedure. As shown in Figure 3, non-uniform grid spacing in both the x and y directions is used.

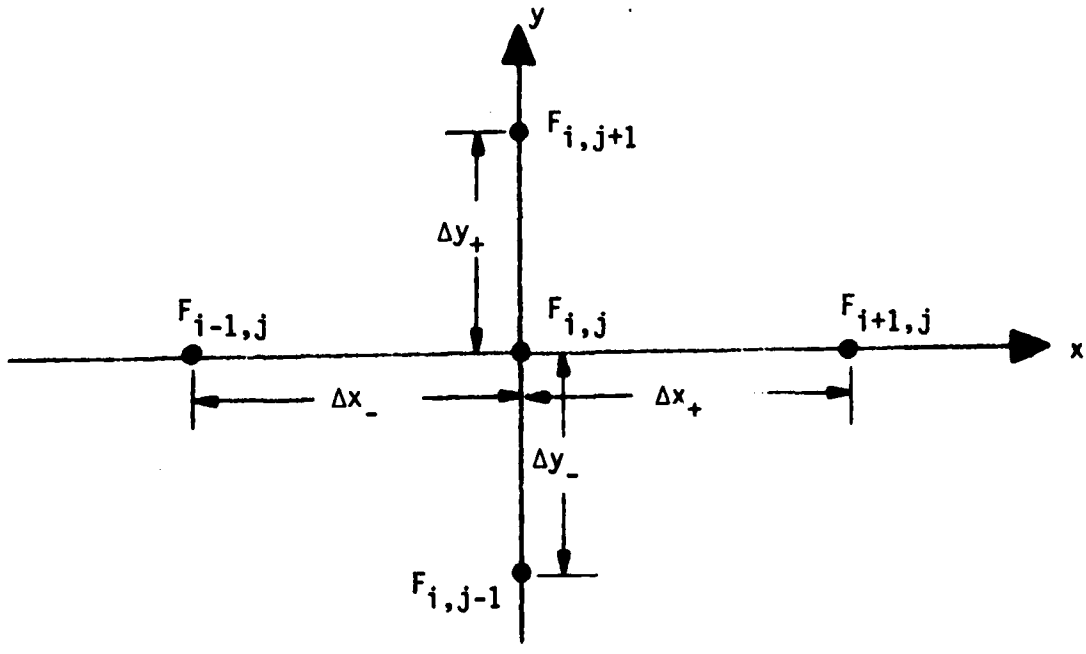

FIGURE 3. FINITE-DIFFERENCE GRID

Values are known at station i and unknown at downstream station i + 1. The equations are solved in an uncoupled manner in the sequence: momentum, continuity, and energy. The finite-difference formulation used depends on the x station. At station 1 there is no x variation. Central differences are used for the y variations at all stations. For example,

$$V \frac{\partial F}{\partial y} = \frac{\hat{V}_j^{i+1}}{(\Delta y_+ + \Delta y_-)}\left[(F_{j+1}^{i+1} - F_j^{i+1}) \frac{\Delta y_-}{\Delta y_+} + (F_j^{i+1} - F_{j-1}^{i+1}) \frac{\Delta y_+}{\Delta y_-}\right] \qquad (28)$$

where $\hat{V}$ denotes the most recent evaluation of V at i+1 level. Unequal grid spacing in the normal direction is implemented by a geometric progression such that the ratio of two adjacent normal coordinate increments is a constant. This ratio was set at 1.08 for the calculations reported here. For the general continuing calculation we want to use information from the two previous stations to obtain second-order accurate representations of the x-derivative terms at the i+1 level and to obtain a second-order accurate representation of the velocities that appear as coefficients in the convective terms. However, for the second calculation station we only have information at one station so we use a more conventional fully implicit scheme. At x station 2, for example,

$$xF \frac{\partial F}{\partial x} = x^{i+1} \hat{F}_j^{i+1} \frac{(F_j^{i+1} - F_j^{i})}{\Delta x_+} \qquad (29)$$

where $\hat{F}_j^{i+1}$ values are taken as known values at the i level initially and updated if iterations are used. It is generally not crucial that they be updated. For all other calculation stations beyond the second, streamwise derivatives are approximated to second-order accuracy by using three-point difference representations. Second-order accuracy for the convective terms is maintained without iterations by the use of extrapolated values of the coefficients. For example,

$$xF \frac{\partial F}{\partial x} = x^{i+1} \, UxT \, (Dx3F_j^{i+1} - Dx2F_j^{i} + Dx1F_j^{i-1}) \qquad (30)$$

where

$$Dx1 = \Delta x_+/(\Delta x_- (\Delta x_+ + \Delta x_-))$$

$$Dx2 = (\Delta x_+ + \Delta x_-)/(\Delta x_+ + \Delta x_-) \tag{31}$$

$$Dx3 = (\Delta x_- + 2\Delta x_+)/(\Delta x_+(\Delta x_+ + \Delta x_-))$$

and

$$UxT = F_j^{i+1} = F_j^i + \frac{(F_j^i - F_j^{i-1})}{\Delta x_-} \Delta x_+ + O(\Delta x)^2 \quad . \tag{32}$$

Note that is the above difference representations, F^2 has been linearized by

$$F^2 = \hat{F}_j^{i+1} F_j^{i+1} \quad . \tag{33}$$

Each difference equation for the momentum and energy equations has three unknowns (F_{j+1}^{i+1}, F_j^{i+1}, F_{j-1}^{i+1}) and can be arranged in the form

$$A_j F_{j-1}^{i+1} + B_j F_j^{i+1} + C_j F_{j+1}^{i+1} = D_j \quad . \tag{34}$$

This system of equations is a tri-diagonal form and is solved efficiently by the Thomas algorithm. It is important to keep $B_j > 0$ and A_j, $C_j < 0$ or unphysical results with wiggles can follow. If $A_j > 0$, the central difference representation, e.g., Equation (28), is replaced by a forward difference

$$V \frac{\partial F}{\partial y} = \hat{V}_j^{i+1} \frac{(F_{j+1}^{i+1} - F_j^{i+1})}{\Delta y_+} \tag{35}$$

and if $C_j > 0$, a backward difference

$$V\frac{\partial F}{\partial y} = \hat{V}_j^{i+1}\frac{(F_j^{i+1} - F_{j-1}^{i+1})}{\Delta y_-} \tag{36}$$

is used. The continuity equation can be solved explicitly for V_j^{i+1}. Several features of the present difference procedure are as described by Harris[16]. For the final closure of equations, the density is obtained from the ideal gas relations

$$\rho_w/\rho = T/T_w, \quad h = c_p T \tag{37}$$

and the molecular viscosity from Sutherland's formula

$$\mu = 2.27 \times 10^{-8}\left(\frac{T^{1/2}}{1 + 198.6/T}\right)\frac{\text{lb sec}}{\text{ft}^2} \quad . \tag{38}$$

The skin friction coefficient is calculated from the smooth wall contribution plus the form-drag contribution

$$c_{fr} = c_{fs} + \frac{1}{2}\int_o^K \frac{u^2 c_D D(y) f(y)}{\rho_e u_e^2 L^2 B(y)}\, dy \quad . \tag{39}$$

Heat transfer coefficients cannot be calculated in a similar manner because there is no heat transfer mechanism analogous to form drag. A simple technique suggested by Finson and Clarke was adopted in this study. That is, the heat transfer augmentation due to roughness is equal to the square root of the skin friction augmentation due to roughness. Physically, this is reasonable because velocity fluctuations are increased by roughness but temperature fluctuations are hardly changed by roughness and $\tau_w \sim \overline{u'v'}$ and $\dot{q}_w \sim \overline{v'T'}$.

SECTION III

DISCUSSION OF RESULTS

Comparisons were made to the smooth and square roughness pattern data taken by Fiore in the AFWAL Mach 6 facility. Profile data were obtained at 17.15 inches from the test plate leading edge for tunnel total pressures of approximately 700, 1400, and 2000 psia and a tunnel total temperature of 1100°R. Both probe and laser velocimeter measurements were taken. Surface pressures and temperatures were also measured along the plate length. A summary of the rms edge and wall conditions for the smooth and rough wall runs are given in Table 1.

TABLE 1. NOMINAL TEST CONDITIONS

CONFIG.	x IN.	M_e	P_o psia	T_o °R	P_w psia	T_w °R	Re/ℓ ft^{-1}	Re_x
SFP	17.20	5.92	1979.78	1086.54	1.36	601.90	2.521×10^7	3.613×10^7
SFP		5.89	1402.54	1078.39	1.00	635.51	1.829×10^7	2.621×10^7
SFP		5.89	703.29	1067.65	0.50	648.69	0.9309×10^7	1.334×10^7
RFP		5.77	2001.03	1131.85	1.61	691.94	2.557×10^7	3.665×10^7
RFP		5.76	1799.68	1125.33	1.47	751.98	2.329×10^7	3.338×10^7
RFP		5.74	1402.99	1120.76	1.17	778.89	1.843×10^7	2.642×10^7
RFP		5.67	704.27	1114.24	0.63	789.64	1.008×10^7	1.445×10^7

(SFP = SMOOTH FLAT PLATE, RFP = ROUGH FLAT PLATE)

Calculations were performed for all three tunnel pressures. Since results are similar, profile comparisons are shown only for P_o = 1400 psia. Figure 4 is a plot of the smooth and rough wall velocity profiles obtained with standard probes and a laser velocimeter (L.V.) method. Both experimental techniques produce profiles that agree very well with each other. This agreement applies to both the smooth and rough models. It should be noted that the velocity profile for the rough flat plate is not as full as that for the smooth flat plate. This is caused by a momentum loss in the flow field around the roughness protuberance resulting from both local shock waves and wakes generated by the protuberances themselves. Predictions are in good agreement with the data for both the smooth and rough surfaces. Symbols represent the data and curves the theory. A value of C_D = 0.6 was used for all rough-wall calculations presented in this report.

Static temperature profile predictions are shown in Figure 5. For a constant value of y/δ the rough surface static temperature ratio is greater than the smooth wall case. For example at y/δ = 0.275 the ratio is 3.45 for the rough wall as compared to 2.50 for the smooth wall case. The smooth wall computations agree reasonably well with the static temperature ratio measurements for $0.3 \leq y/\delta \leq 1.0$; however in the range for $0 \leq y/\delta \leq 0.3$ the computations underpredict the measured values of T/T_e. This may be a problem with locating the temperature edge value in the computer code. Temperature results near the wall are sensitive to the procedure for defining the temperature edge conditions. Rough wall results look good but this may be fortuitous in light of the smooth wall results. It should be noted that very near the wall the theory indicates a peak in T/T_e. This peak was not noted in the experimental data simply because the probe size did not permit obtaining data in the region $0 \leq y/\delta \leq 0.07$. The peak predicted for the rough wall may be too high, because an increase in the rough wall mixing length near the wall for the momentum equation results in a corresponding increase in the temperature calculated from the energy equation. However, for a rough surface heat transfer around the roughness elements is principally by molecular conduction.

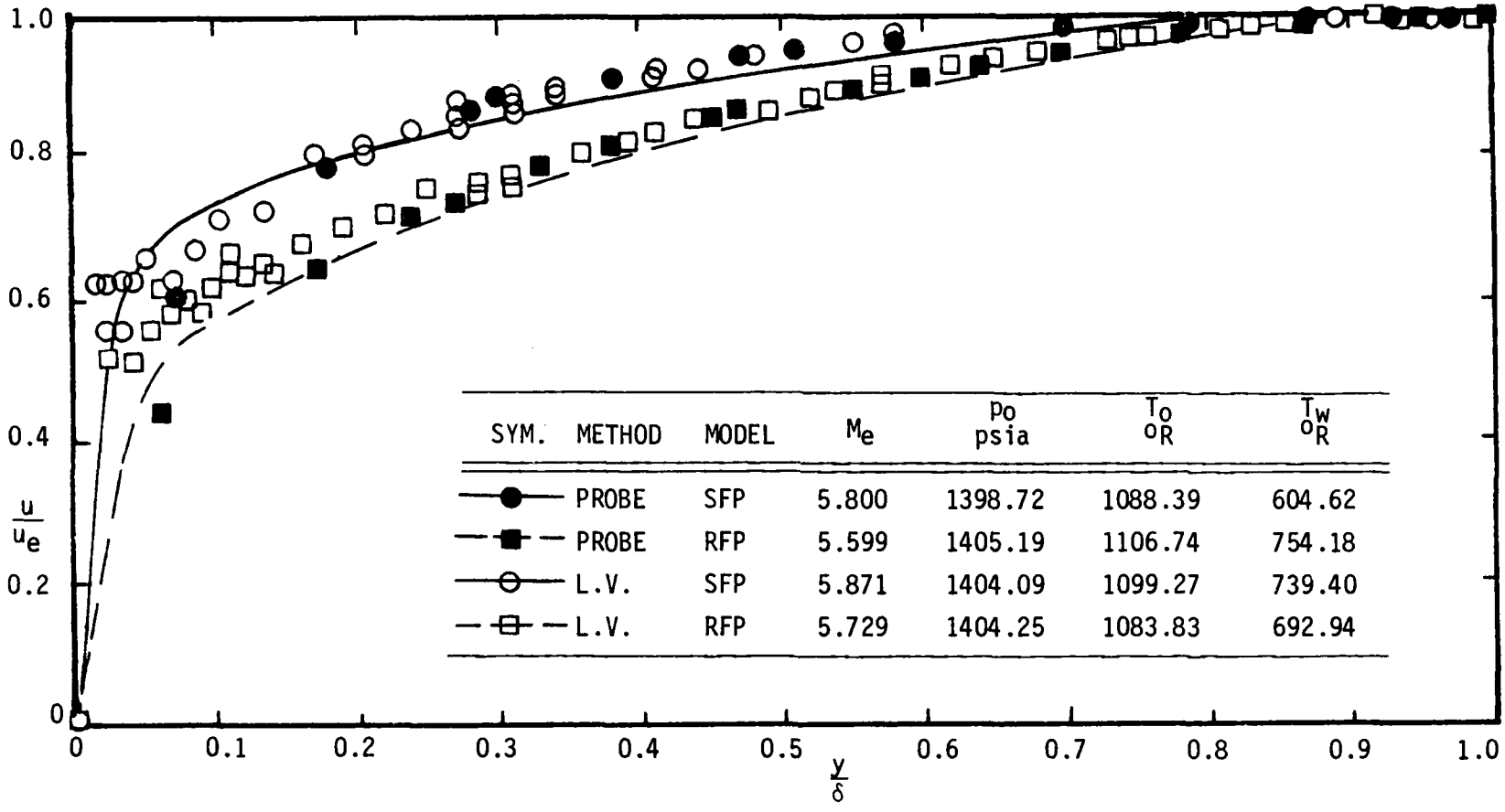

FIGURE 4. VELOCITY DISTRIBUTION AT X = 17.15 INCHES

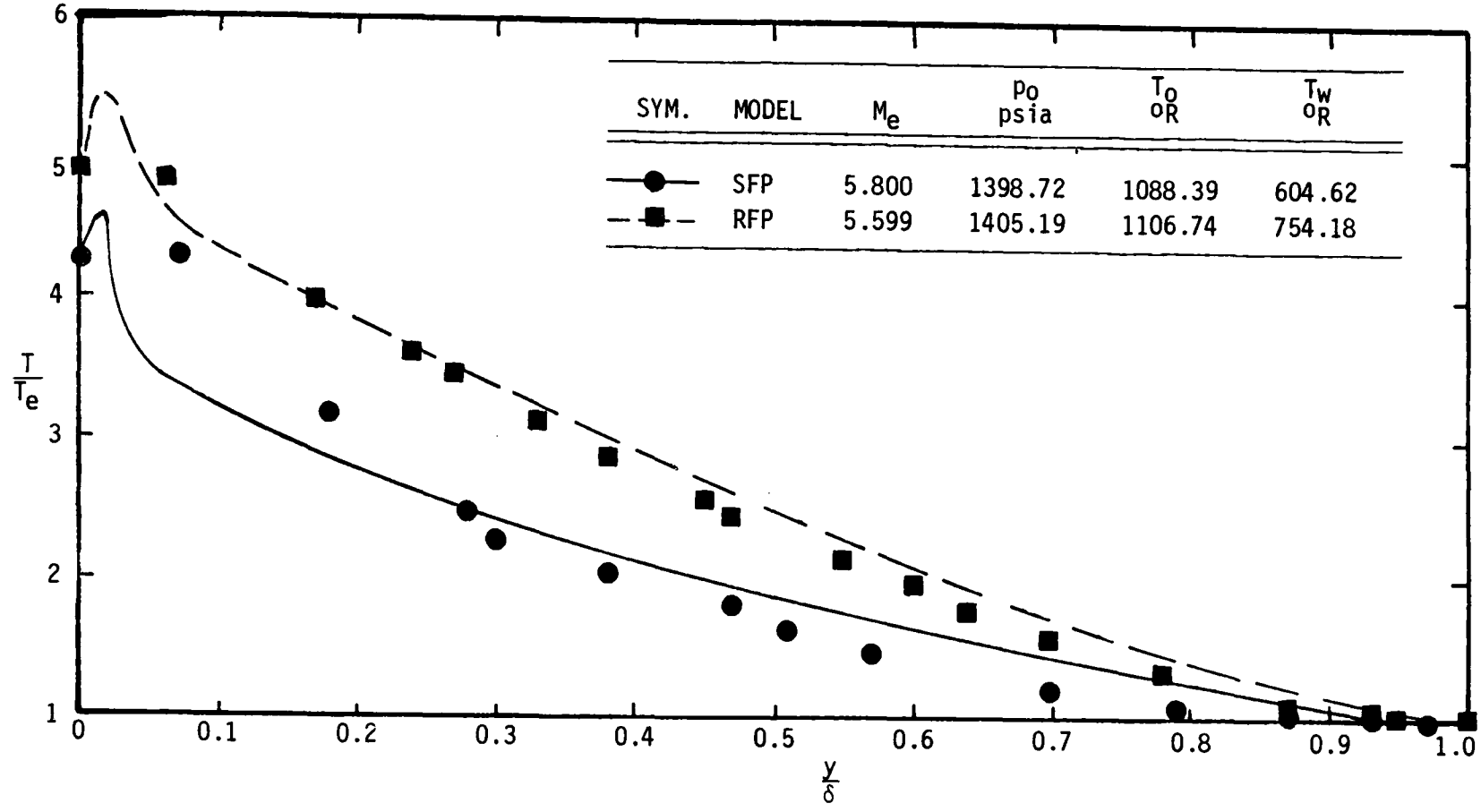

FIGURE 5. STATIC TEMPERATURE DISTRIBUTION AT X = 17.15 INCHES (PROBE DATA)

Underprediction of the smooth wall static temperature near the plate surface, along with slight discrepancies in the velocity predictions, results in the total temperature being underpredicted. This is shown in Figure 6. Again, rough wall values look good. Basically the local total temperature measurements are the same for both the smooth and rough flat plates. The computations also indicate that the temperature distribution is relatively invariant with roughness. The local Mach number distribution is presented in Figure 7. In general the local Mach number for the rough surface is lower than the smooth wall case. This is believed to be due to a decrease in momentum caused by the roughness protuberances. For both the smooth and rough walls, the Mach number in the outer part of the boundary layer is underpredicted because the static temperature is overpredicted and the velocity is slightly underpredicted.

The Pitot pressure through the boundary layer is presented in Figure 8. The measurements indicate that the local Pitot pressures for the rough flat plate are everywhere less than the smooth flat plate case. The computations agree reasonably well with the measurements for both the smooth and rough flat plates, except in the outer region where the Mach number calculations disagree.

Figure 9 is interesting, but not as dramatic as results for P_0 = 2000 psia. The smooth and rough wall data collapse on the same curve when T/T_e is plotted against u/u_e. (Note that the differences shown in Figure 9 result from very different values of T_w/T_e for the smooth and rough wall runs.) This implies that a Crocco type approximation is valid for rough surfaces, even at Mach 6.

Skin friction coefficients were obtained by Fiore using both a Preseton tube and by iterating on "law of the wall" velocity profiles. In the smooth wall case the Preston tube values were used while the iterative skin friction coefficients for the rough wall are reported. These results, along with predictions, are shown in Table 2. Predictions are in very good agreement with the data, except for the rough surface at P_0 = 2000 psia. The data show an increase in c_f in going from P_0 = 1400 psia to P_0 = 2000 psia while the

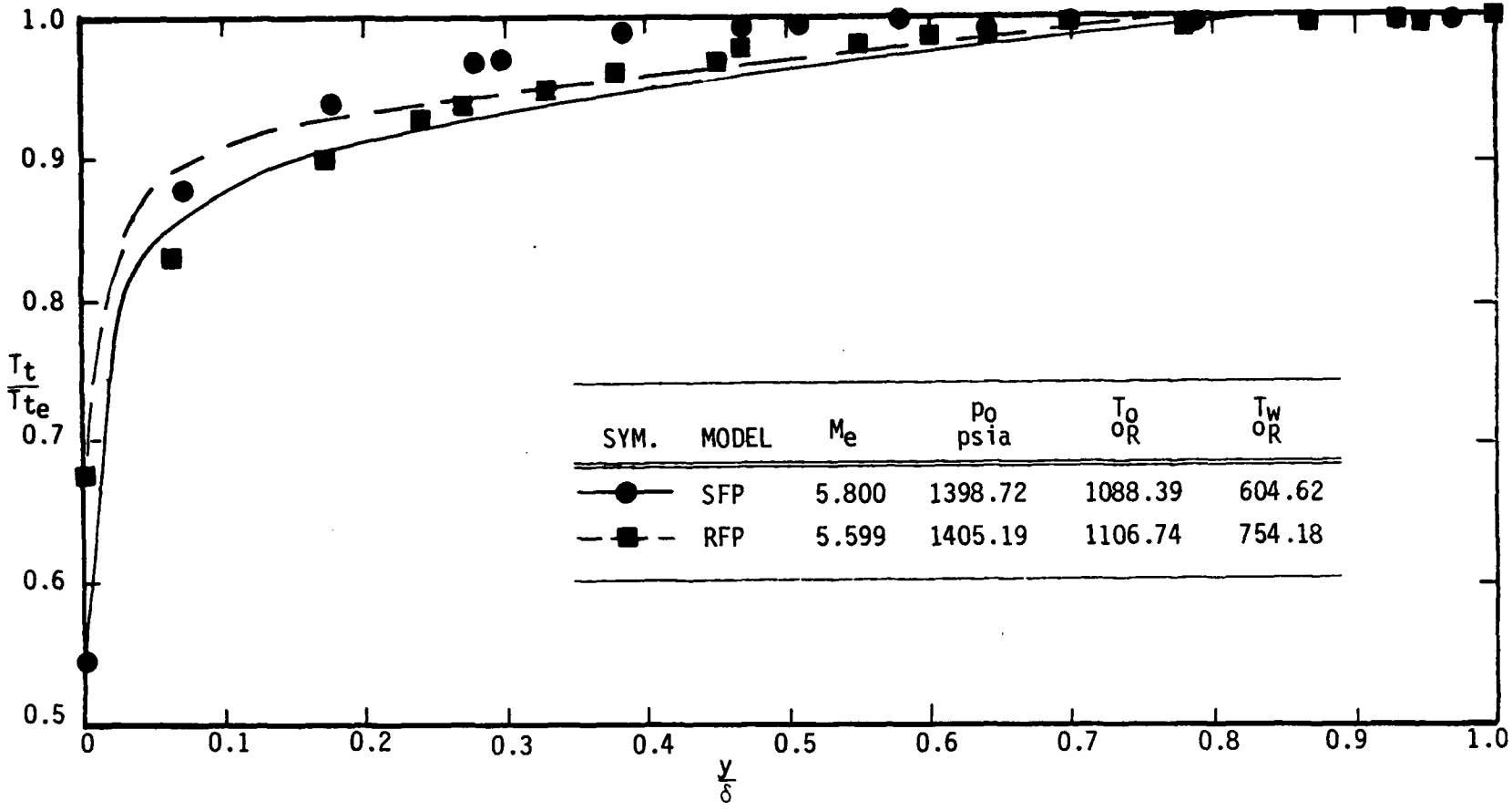

FIGURE 6. TOTAL TEMPERATURE DISTRIBUTION AT X = 17.15 INCHES (PROBE DATA)

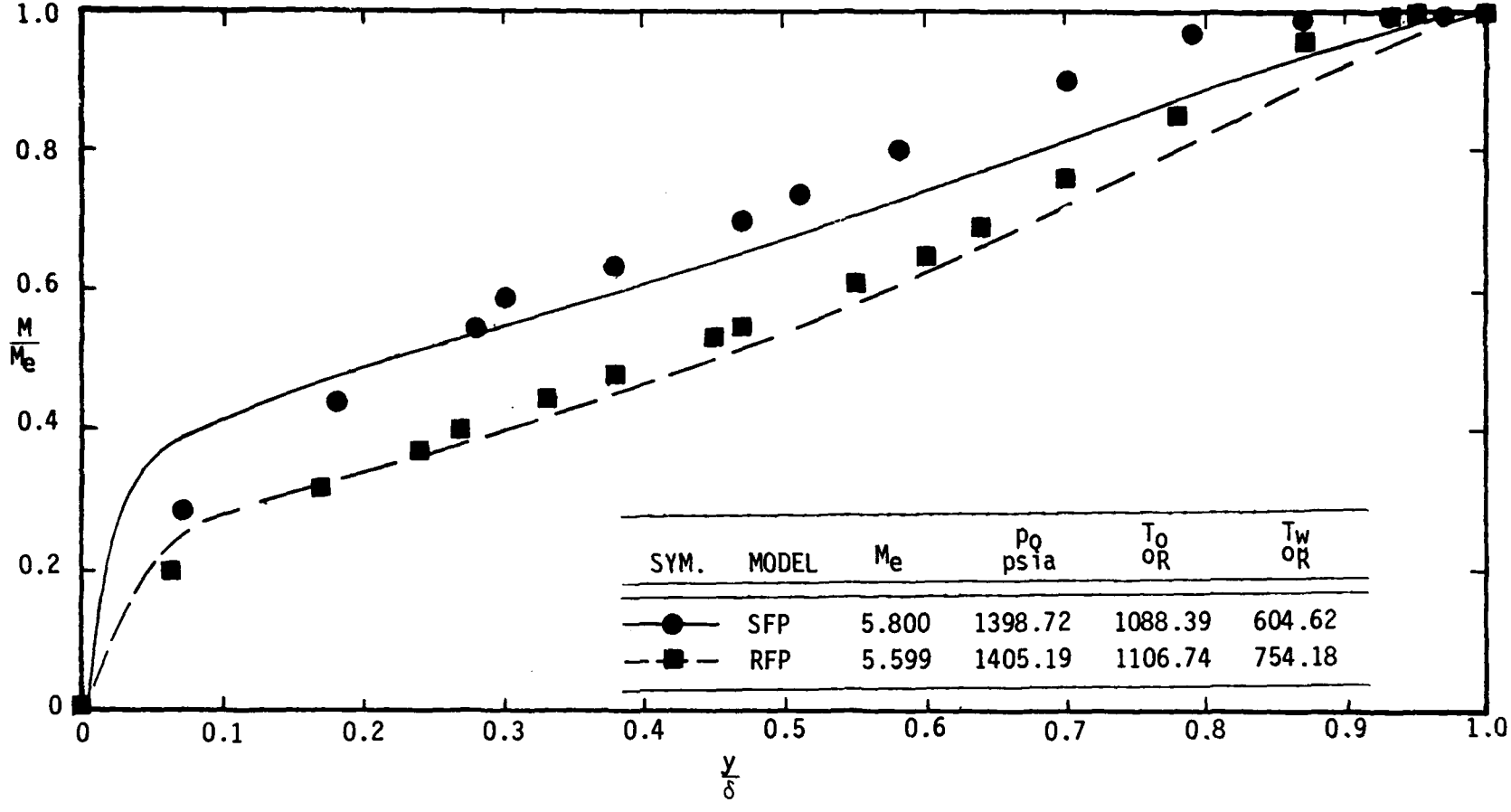

FIGURE 7. MACH NUMBER DISTRIBUTION AT X = 17.15 INCHES (PROBE DATA)

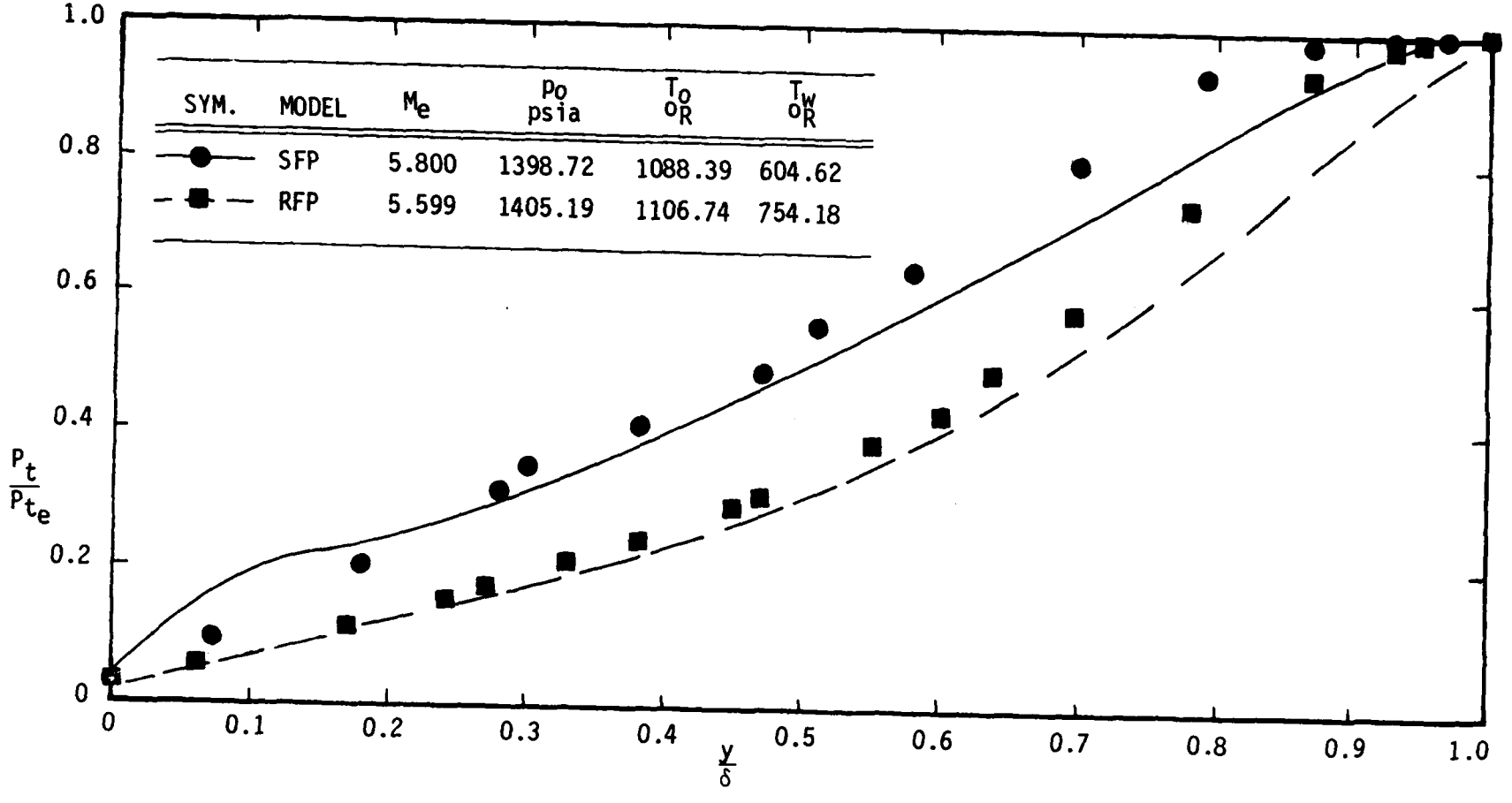

FIGURE 8. TOTAL PRESSURE DISTRIBUTION AT X = 17.15 INCHES (PROBE DATA)

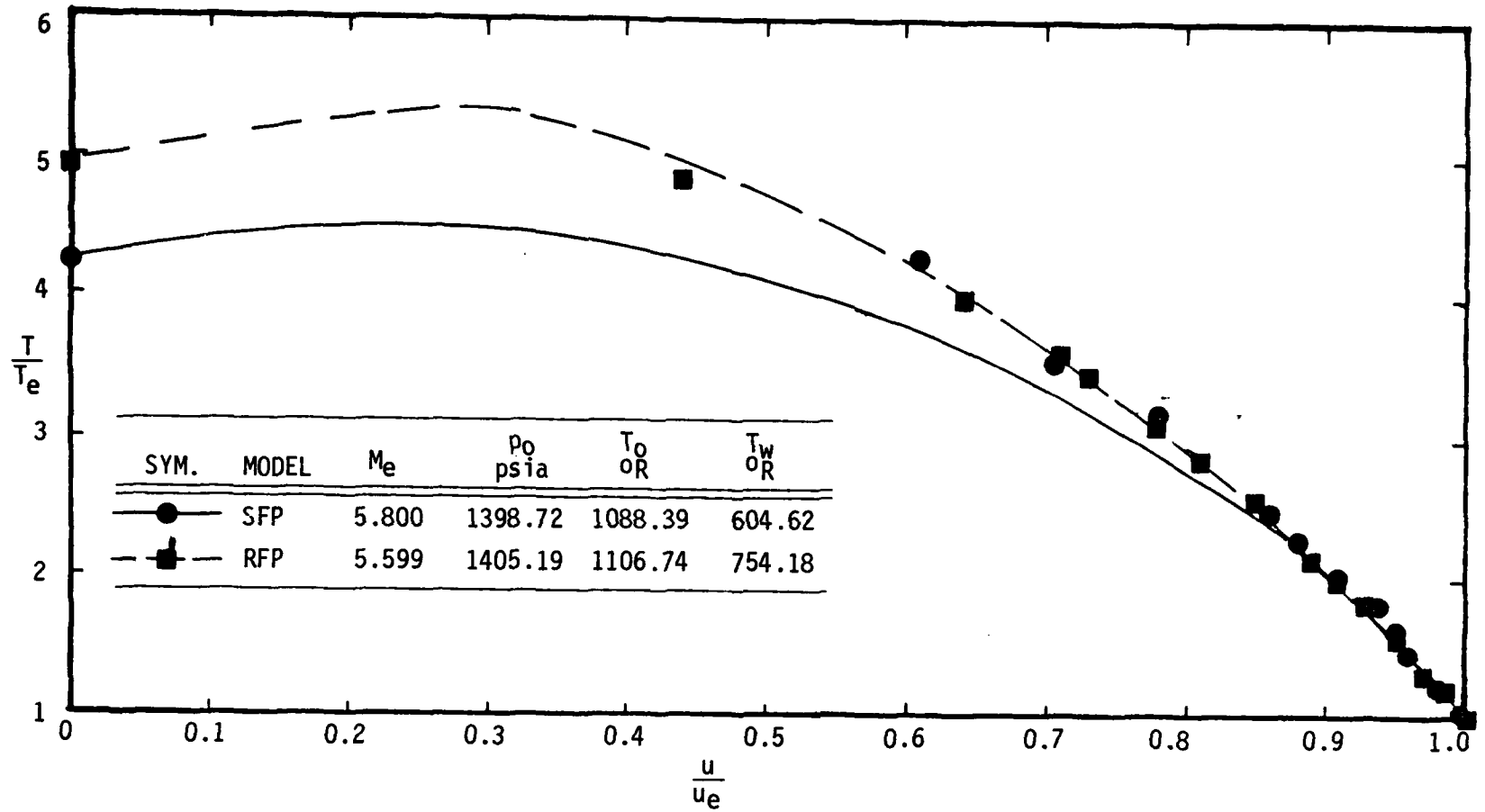

FIGURE 9. T/T_E VERSUS u/u_E AT X = 17.15 INCHES (PROBE DATA)

TABLE 2. SKIN FRICTION COEFFICIENT COMPARISONS AT x = 17.15 INCHES

CONFIGURATION	M_e	p_o psia	T_o °R	T_w °R	$c_f \times 10^3$ (Experiment)	$c_f \times 10^3$ (Theory)
SFP	5.72	701.45	1080.03	604.62	1.202	1.131
SFP	5.80	1398.72	1088.39	604.62	1.002	1.000
SFP	5.94	1995.38	1098.60	664.62	0.898	0.910
RFP	5.44	705.61	1098.49	764.37	1.654	1.543
RFP	5.60	1405.19	1106.74	754.18	1.347	1.368
RFP	5.53	2003.53	1122.94	654.52	1.622	1.363

predictions show a leveling off. It should be noted that the experimental rough wall c_f values may not be very accurate because of the dearth of data in the log portion of the profiles.

It should also be mentioned that the predicted smooth wall values of the boundary layer thicknesses are in good agreement with the experimental data. While both the measured and calculated rough wall boundary layer thicknesses were found to be essentially independent of Reynolds number, the magnitudes were quite different ($\delta_{exp.}$ = 0.38 inches and δ_{theory} = 0.52 inches).

Finally, in the calculations reported above, shocks were assumed weak ($M \sin \theta = 1.025$). This gave shock shapes that appeared similar to Schlieren obtained by Fiore. Calculations were also made without shocks. There was no discernible effect of the shocklets for Mach number, total temperature, and total pressure distributions. Near the wall, slight shock effects were noticed for velocity and static temperature distributions. With the shocks, u/u_e decreased less than 4 percent for $y/\delta < 0.2$ and T/T_e increased less than 2 percent for $y/\delta < 0.5$. Outside of these y/δ ranges, u/u_e and T/T_e were essentially unchanged. For the case of tunnel total pressure of 1400 psia, modeling the shocks in the calculations increased the boundary layer thickness by 2.5 percent and decreased the skin friction coefficient by 1 percent.

SECTION IV

CONCLUSIONS/RECOMMENDATIONS

The fully implicit finite-difference boundary layer procedure of Christoph and Pletcher[10] for flow over rough surfaces has been extended to include the effect of shocks off the roughness elements. The method employs a two-layer algebraic mixing-length model that explicitly accounts for roughness height, spacing, and geometry. The equivalent sand-grain concept is not used. Oblique shock relations are used to calculate flow conditions through the boundary layer behind each shock.

Computations are presented for smooth and rough wall data obtained at AFWAL . In general, the agreement between experiment and theory is very good. The smooth wall static temperature predictions are in disagreement with the data near the surface. It is felt that this could be a problem with the code search procedure for T_e, and not with turbulence modeling. Also, for both the smooth and rough plates, the theory predicts a maximum temperature near the wall that is not captured by the measurements. Smooth wall skin friction coefficients agree very well with the data. The rough wall skin friction predictions are encouraging, even though the accuracy of the skin friction coefficients obtained from the rough wall profiles is uncertain.

Several extensions/improvements to the method described in this report are suggested. These are:

(1) Higher order turbulence models should be used. Possibilities are a lag equation model and a turbulence kinetic energy - turbulence dissipation rate (k-ε) model.

(2) Mass addition should be added as a boundary condition and in the turbulence model so that coupled roughness/blowing effects can be examined.

(3) From other data comparisons, it has been observed that the code of Christoph and Pletcher[10] does not accurately predict rough wall heat transfer. The reason is that an increase in the mixing-length for the momentum equation results in an increase in the heat transfer calculated from the energy equation. However, for a rough surface heat transfer near the wall is principally by molecular conduction. A conduction sublayer model within the framework of the above analysis is needed.

REFERENCES

1. D. Betterman, "Contribution a l'Etude de la Connection Forces Turbulente le Long de Plaques Rugueuses," Int. J. Heat & Mass Transfer, Vol. 9, 1966, pp. 153-164.

2. R. B. Dirling, Jr., "A Method for Computing Roughwall Heat Transfer Rates on Re-entry Nosetips," AIAA Paper No. 73-763, presented at the AIAA 8th Thermophysics Conference, Palm Springs, Calif., July 16-18, 1973.

3. C. O. White and R. M. Grabow, "Nosetip Design Technology Program Final Report, Vol. I, Pattern Roughness Methodology," SAMSO-TR-75-70, March 1975.

4. T. Cebeci, and K, C. Chang, "Calculation of Incompressible Rough-Wall Boundary-Layer Flows," AIAA Journal, Vol. 16, No. 7, July 1978, pp. 730-735.

5. J. C. Rotta, "Turbulent Boundary Layers in Incompressible Flow," Progress in Aerospace Science, Vol. 2, 1962, pp. 1-219.

6. B. K. Hodge, and J. C. Adams, "The Calculation of Compressible Turbulent, and Relaminarization Boundary Layers Over Smooth and Rough Surfaces Using an Extended Mixing-Length Hypothesis," AEDC-TR-77-96, February 1978.

7. J. M. Healzer, R. J. Moffat, and W. M. Kays, "TheTurbulent Boundary Layer on a Porous Rough Plate: Experimental Heat Transfer with Uniform Blowing," AIAA Paper No. 74-680 and ASME Paper No. 74-HT-14, presented at the AIAA/ASME 1974 Thermophysics and Heat Transfer Conference, Boston, Massachusetts, July 15-17, 1974.

8. M. L. Finson and A. S. Clarke, "The Effect of Surface Roughness Character on Turbulent Re-entry Heating," AIAA Paper No. 80-1459, 1980.

9. T. C. Lin and R. J. Bywater, "Turbulence Models for High-Speed, Rough-Wall Boundary Layers," AIAA Journal, Vol. 20, No. 3, March 1982, pp.325-333.

10. G. H. Christoph and R. H. Pletcher, "Prediction of Rough-Wall Skin Friction and Heat Transfer," AIAA Paper No. 82-0031, presented at AIAA 20th Aerospace Sciences Meeting, Orlando, Florida, January 11-14, 1982.

11. E. R. van Driest, "On Turbulent Flow Near a Wall," J. Aero. Sci., Vol. 23, 1956, pp. 1007-1011.

12. R. H. Pletcher, "Prediction of Transpired Turbulent Boundary Layers," Journal of Heat Transfer, Vol. 96, Feb. 1974, pp. 89-94.

13. F. M. White and G. H. Christoph, "A Simple Theory for the Two-Dimensional Compressible Turbulent Boundary Layer," J. Basic Engineering, ASME Trans., Sept. 1972, pp. 636-642.

14. H. Schlichting, "Experimental Investigation of the Problem of Surface Roughness," NACA TM823 (1937). Also Boundary Layer Theory, McGraw-Hill, New York 1968.

15. R. H. Pletcher, "Prediction of Turbulent Boundary Layers at Low Reynolds Numbers," AIAA Journal, Vol. 14, 1976, pp. 696-698.

16. J. E. Harris, "Numerical Solution of the Equations for Compressible, Laminar, Transitional, and Turbulent Boundary Layers and Comparisons with Experimental Data," NASA TR R-368, 1971.

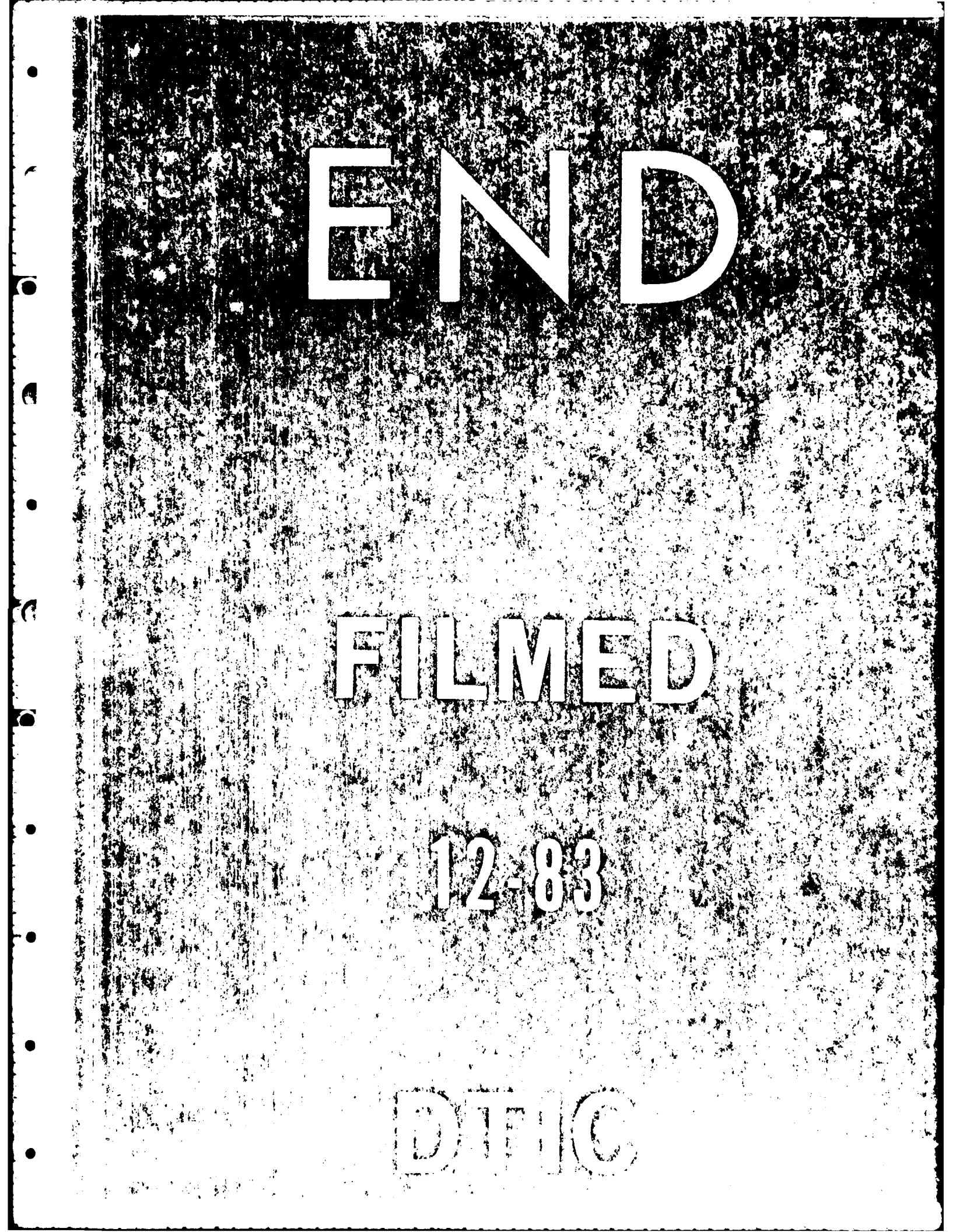
END
FILMED
12-83
DTIC